Chinese Journal of Aeronautics, (2015),28(1): 305–313

Chinese Society of Aeronautics and Astronautics
& Beihang University

Chinese Journal of Aeronautics

cja@buaa.edu.cn
www.sciencedirect.com

Active vibration control of piezoelectric bonded smart structures using PID algorithm

Zhang Shunqi [a,b,*], Rüdiger Schmidt [b], Qin Xiansheng [a]

[a] School of Mechanical Engineering, Northwestern Polytechnical University, Xi'an 710072, China
[b] Institute of General Mechanics, RWTH Aachen University, Aachen 52062, Germany

Received 27 May 2014; revised 2 July 2014; accepted 25 August 2014
Available online 24 December 2014

KEYWORDS

Smart structures;
Active vibration control;
PID control;
Piezoelectric;
Finite element

Abstract Thin-walled structures are sensitive to vibrate under even very small disturbances. In order to design a suitable controller for vibration suppression of thin-walled smart structures, an electro-mechanically coupled finite element (FE) model of smart structures is developed based on first-order shear deformation (FOSD) hypothesis. Considering the vibrations generated by various disturbances, which include free and forced vibrations, a PID control is implemented to damp both the free and forced vibrations. Additionally, an LQR optimal control is applied for comparison. The implemented control strategies are validated by a piezoelectric layered smart plate under various excitations.

1. Introduction

Due to light-weight design, thin-walled structures are increasingly applied in many fields of technology. Even though there are many beneficial properties that can be derived, many negative effects, e.g. low damping and high vibration sensibility, will be brought into the system as well.

One promising solution is to make the structure smart using piezoelectrics, electrostrictives, magnetostrictives, etc., for active vibration control. In order to avoid high costs of experimental investigations, both theoretical models of smart structures and control strategies are necessary. The most accurate models are derived based on 3-dimensional (3D) solid mechanics, see e.g. Ref. [1–5] among others.

Due to small dimension of thickness, 1-dimensional (1D) FE models based on Bernoulli beam theory[6,7] and Timoshenko beam theory[8,9], and 2-dimensional (2D) models based on Kirchhoff–Love theory which is called classical theory[10–12] and Reissner–Mindlin theory known as first-order shear deformation (FOSD) theory, e.g. in Ref. [13–17] for linear FE models, and Ref. [18–20] for nonlinear FE models, are much more effective, compared to 3D FE models. Shimpi and Patel[21] presented a model of two variable refined plate theory, which has a strong similarity to the classical plate theory.

With the linear displacement distribution, FOSD hypothesis is applicable for thin to moderate thick plates and shells. In order to deal with thick structures, third-order shear deformation (TOSD) or higher-order shear deformation (HOSD)

* Corresponding author at: School of Mechanical Engineering, Northwestern Polytechnical University, Xi'an 710072, China. Tel.: +86 029 88494271.
E-mail addresses: sqzhangnpu@mail.nwpu.edu.cn, shunqi.zhang@hotmail.com (S. Zhang).

Peer review under responsibility of Editorial Committee of CJA.

Production and hosting by Elsevier

http://dx.doi.org/10.1016/j.cja.2014.12.005

hypotheses have been firstly proposed by Reddy[22] for composite structures. Later the theory was extended and developed by Hanna and Leissa,[23] Correia et al.,[24] Moita et al.,[25] Schmidt and Vu[26] for smart structures. Additionally, Vasques and Rodrigues[27] applied layerwise shear deformation theory, while, Kapuria et al.[28,29] developed third-order zigzag shear deformation theory.

Concerning control method for vibration suppression of smart structures, the majority of papers in the literature presented negative velocity feedback control using FE models based on various hypotheses, e.g. classical plate theory,[10,12,30,31] Timoshenko beam theory,[8] FOSD hypothesis,[14,32–35] TOSD hypothesis,[25] HOSD hypothesis,[36] first-order zigzag hypothesis[37,38] and by using commercial software.[39] In addition, Liu et al.[16] implemented the same control law but using a mesh-free model based on the FOSD hypothesis. Furthermore, Kang et al.[31] implemented a negative velocity feedback control into a real smart beam experimentally for vibration control. Apart from negative velocity feedback control law, Narayanan and Balamurugan,[8] as well as Balamurugan and Narayanan[32] implemented a Lyapunov feedback control for active vibration control of smart structures based on the models obtained by the FOSD hypothesis. Tzou and Chai[6] applied bang-bang control numerically based on Euler–Bernoulli beam theory, and they also carried out the control schemes experimentally.

Optimal control laws are very popular in the simulation of vibration suppression of smart structures. Numerous papers can be found in the literature in which Linear Quadratic Regulator (LQR) control with FE models were developed based on e.g. classical plate/shell theory,[31] Timoshenko beam theory,[8] FOSD hypothesis,[32,40] layerwise theory,[38] 3D solution[41] and others.[42] Since LQR control is a full state feedback control, all state variables have to be measured, which cannot be implemented into real systems in most of the cases. Therefore, Linear Quadratic Gaussian (LQG) control was implemented by Vasques and Rodrigues[36] numerically and by Dong et al.[43] both numerically and experimentally, in which the state variables were estimated by using measured signals. Additionally, Stavroulakis et al.[44] implemented LQR control and robust H_2 control into the model derived based on Euler–Bernoulli beam theory, and they compared the results with each other. Marinaki et al.[9] developed a particle swarm optimization-based controller for vibration suppression of beams. Moreover, Roy and Chakraborty[45] proposed a genetic algorithm-based LQR control for smart fiber reinforced polymer composite shell structures using the model derived by Bernoulli beam theory.

Some other advanced control schemes can also be found in the literature. Chen and Shen,[46] as well as Lin and Nien[47] presented an independent modal space control for vibration suppression of smart structures, while, Bhattacharya et al.[48] proposed an independent modal space control-based LQR control strategy for vibration control of laminated spherical shell with different fiber orientation and varying radius of curvature based on Reissner's hypothesis. Furthermore, Manjunath and Bandyopadhyay[49] proposed a discrete sliding mode control scheme with Timoshenko beam theory for the vibration control of smart flexible beams. A prediction control algorithm was applied by Valliappan and Qi[41] and a disturbance rejection control was designed by Zhang et al.[50] for vibration control of piezoelectric patches bonded beams. In addition, robust control has been considered by Li et al.,[51] as well as Marinova et al.[52]

From the literature cited above, most of them developed simple mathematical models based on e.g. Euler–Bernoulli beam theory, Timoshenko beam theory, classical plate theory and FOSD theory used for control design. In those papers which used FE models based on refined theories usually additional simplifications are introduced e.g. the neglect of strain components which are distributed quadratically along the thickness direction. One of the purposes of this paper is to construct a FE model based on FOSD hypothesis without neglecting any strain components. Secondly, the majority of published papers only considered the free vibration case which has no steady-state error. The most frequently used control strategies, e.g. velocity feedback, LQR, etc., can damp the free vibrations successfully. However, they cannot counteract the steady-state error generated by a disturbance force. Therefore, a PID control is developed and applied to counteract both the free vibration and the steady-state error for the structure under a disturbance force.

2. Dynamic FE model

In order to derive a dynamic FE model of a smart structure, two coordinate systems are introduced, namely, the Cartesian coordinate system represented by $X_i (i = 1,2,3)$ as global coordinates and the curvilinear coordinate system denoted by $\theta_i (i = 1,2,3)$, which can be cylindrical, spherical or any other coordinates, as shown in Fig. 1.

The left part of the figure shows the structure in the undeformed configuration, while the right part indicates the deformed configuration. The quantities with over bar $\bar{\square}$ represent those in the deformed configuration. In the figure, $\boldsymbol{u}$ represents the displacement vector of an arbitrary point P_V in the shell space and $\boldsymbol{u}^0$ the displacement of an arbitrary point P_Ω at the mid-surface. Introducing a rotation vector $\boldsymbol{u}^1$ of the shell director, which is defined as $\boldsymbol{u}^1 = \bar{\boldsymbol{a}}_3 - \boldsymbol{n}$, $\boldsymbol{n}$ is the base vector in θ_3 direction in the undeformed configuration, and $\bar{\boldsymbol{a}}_3$ is the base vector in the deformed configuration, one obtains the expression of the displacement vector in the shell space based on the FOSD hypothesis as

$$\boldsymbol{u} = \boldsymbol{u}^0 + \theta_3 \boldsymbol{u}^1 \tag{1}$$

with

$$\boldsymbol{u} = \begin{bmatrix} v_1 \\ v_2 \\ v_3 \end{bmatrix}, \quad \boldsymbol{u}^0 = \begin{bmatrix} v_1^0 \\ v_2^0 \\ v_3^0 \end{bmatrix}, \quad \boldsymbol{u}^1 = \begin{bmatrix} v_1^1 \\ v_2^1 \\ 0 \end{bmatrix} \tag{2}$$

Here, v_1, v_2, v_3 denote the displacements in the shell space, v_1^0, v_2^0, v_3^0 are the translational displacements at the mid-surface,

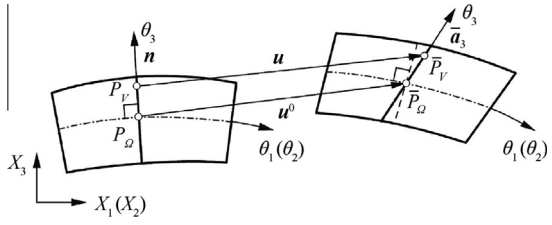

Fig. 1 Displacement distribution in thickness direction according to the FOSD hypothesis.

and v_1^1, v_2^1 are the mid-surface rotational displacements, which are called five parameters of the FOSD theory. In Eq. (1), θ_3 represents the distance between point P_V and the mid-surface. Furthermore, Eq. (1) can be expressed as

$$\boldsymbol{u} = \boldsymbol{Z}_{\mathrm{u}} \begin{bmatrix} \boldsymbol{u}^0 \\ \boldsymbol{u}^1 \end{bmatrix} \tag{3}$$

where matrix Z_{u} is composed of θ_3 (the details can be found in Ref. [19]).

Based on the predefined base vectors and the FOSD hypothesis, the Green–Lagrange strain tensor of the in-plane $\varepsilon_{\alpha\beta}$ and the transverse shear $\varepsilon_{\alpha 3}$ components can be obtained as (for more detailed information please refer to Ref. [19,20,53])

$$\begin{cases} \varepsilon_{\alpha\beta} = \varepsilon^0_{\alpha\beta} + \theta_3 \varepsilon^1_{\alpha\beta} + (\theta_3)^2 \varepsilon^2_{\alpha\beta} \\ \varepsilon_{\alpha 3} = \varepsilon^0_{\alpha 3} \end{cases} \tag{4}$$

For geometrically linear plate and shell theory the strain terms in the above equations are

$$\begin{cases} 2\varepsilon^0_{\alpha\beta} = \varphi^0_{\alpha\beta} + \varphi^0_{\beta\alpha} \\ 2\varepsilon^1_{\alpha\beta} = v^1_{\alpha|\beta} - b^{\lambda}_{\beta}\varphi^0_{\lambda\alpha} + v^1_{\beta|\alpha} - b^{\delta}_{\alpha}\varphi^0_{\delta\beta} \\ 2\varepsilon^2_{\alpha\beta} = -b^{\lambda}_{\beta} v^1_{\lambda|\alpha} - b^{\delta}_{\alpha} v^1_{\delta|\beta} \\ 2\varepsilon^0_{\alpha 3} = v^1_{\alpha} + v^0_{3,\alpha} + b^{\delta}_{\alpha} v^0_{\delta} \end{cases} \tag{5}$$

with

$$\begin{cases} \varphi^0_{\lambda\alpha} = v^0_{\lambda|\alpha} - b_{\lambda\alpha} v^0_3 \\ v^n_{\lambda|\alpha} = v^n_{\lambda,\alpha} - \Gamma^{\delta}_{\lambda\alpha} v^n_{\delta} \end{cases} \tag{6}$$

Here $b_{\lambda\alpha}$ and b^{λ}_{α} are the covariant and mixed components of the curvature tensor, and $\Gamma^{\delta}_{\lambda\alpha}$ represents the Christoffel symbols of the second kind. Furthermore, $()_{|\alpha}$ and $()_{,\alpha}$ denote respectively the covariant and spatial derivatives with respect to θ_α. The Greek indices represent the numbers 1 or 2, the right superscript n assumes 0 or 1.

Due to the assumption of small strains, linear piezoelectric coupled constitutive equations are considered, which are given by

$$\begin{cases} \boldsymbol{\sigma} = \boldsymbol{c}\boldsymbol{\varepsilon} - \boldsymbol{e}^{\mathrm{T}}\boldsymbol{E} \\ \boldsymbol{D} = \boldsymbol{e}\boldsymbol{\varepsilon} + \boldsymbol{\chi}\boldsymbol{E} \end{cases} \tag{7}$$

where ε, σ, $\boldsymbol{E}$ and $\boldsymbol{D}$ are the Green–Lagrange strain vector, the second Piola–Kirchhoff stress vector, the electric field vector and the electric displacement vector, respectively. Additionally, $\boldsymbol{c}$, $\boldsymbol{e}$ and $\boldsymbol{\chi}$ denote the elasticity matrix, the piezoelectric constant matrix and the dielectric constant matrix, respectively, in which $\boldsymbol{e} = \boldsymbol{dc}$. Concerning the details of all the matrices, one could refer to Ref. [19].

In order to represent the five parameters, we introduce five nodal degrees of freedom (DOFs) including three translational DOFs (u, v, w) and two rotational DOFs (φ_1, φ_2), as displayed in Fig. 2, where a_α represents the covariant base vectors with respect to θ_α.

Consequently, the strain vector can be expressed by element nodal DOF vector $\boldsymbol{q}$ as

$$\boldsymbol{\varepsilon} = \boldsymbol{B}_{\mathrm{u}}\boldsymbol{q} \tag{8}$$

in which B_{u} is the strain field matrix.

Since weak electric potential applied on piezoelectric material is considered, the electric field is assumed to be constant through the thickness direction, which can be expressed by

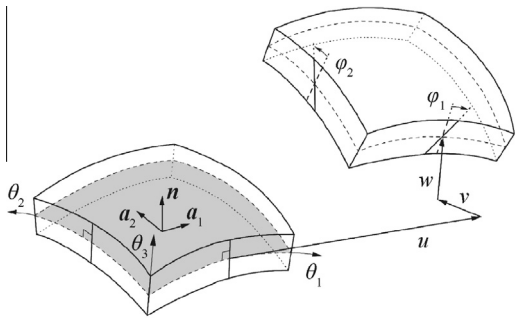

Fig. 2 Nodal degrees of freedom.

$$\boldsymbol{E} = -\nabla\boldsymbol{\phi} = \boldsymbol{B}_{\phi}\boldsymbol{\phi} \tag{9}$$

where ∇ represents the gradient operator, $\boldsymbol{B}_{\phi}$ the electric field matrix, and $\boldsymbol{\phi}$ the electric voltage vector on piezoelectric patches.

In order to obtain the dynamic model, Hamilton's principle is employed, which is described as that the integral of virtual energy over time t_1 to t_2 is equal to 0, given by

$$\int_{t_1}^{t_2} (\delta T - \delta W_{\mathrm{int}} + \delta W_{\mathrm{ext}})\, \mathrm{d}t = 0 \tag{10}$$

Here δ represents the variational operator; δT, δW_{int} and δW_{ext} denote the variation of the kinetic energy, the internal work and the external work and are expressed as

$$\begin{cases} \delta T = -\int_V \rho \delta \boldsymbol{u}^{\mathrm{T}} \ddot{\boldsymbol{u}}\, \mathrm{d}t \\ \delta W_{\mathrm{int}} = \int_V (\delta\boldsymbol{\varepsilon}^{\mathrm{T}}\boldsymbol{\sigma} - \delta\boldsymbol{E}^{\mathrm{T}}\boldsymbol{D})\, \mathrm{d}V \\ \delta W_{\mathrm{ext}} = \int_V \delta\boldsymbol{u}^{\mathrm{T}}\boldsymbol{f}_{\mathrm{b}}\, \mathrm{d}V + \int_{\Omega} \delta\boldsymbol{u}^{\mathrm{T}}\boldsymbol{f}_{\mathrm{s}}\, \mathrm{d}\Omega + \delta u^{\mathrm{T}}\boldsymbol{f}_{\mathrm{c}} \end{cases} \tag{11}$$

where $\boldsymbol{f}_{\mathrm{b}}$, $\boldsymbol{f}_{\mathrm{s}}$ and $\boldsymbol{f}_{\mathrm{c}}$ are the vectors of body, surface and concentrated force, and Ω, V represent the mid-surface area and volume space. Substituting Eq. (11) into Eq. (10) and considering the linear strain–displacement relations, one obtains a linear electro-mechanically coupled dynamic FE model, including the equation of motion and the sensor equation, which are given as[50]

$$\begin{cases} \boldsymbol{M}_{\mathrm{uu}}\ddot{\boldsymbol{q}} + \boldsymbol{C}_{\mathrm{uu}}\dot{q} + \boldsymbol{K}_{\mathrm{uu}}\boldsymbol{q} + \boldsymbol{K}_{\mathrm{u}\phi}\boldsymbol{\phi}_{\mathrm{a}} = \boldsymbol{F}_{\mathrm{ue}} \\ \boldsymbol{K}_{\phi\mathrm{u}}\boldsymbol{q} + \boldsymbol{K}_{\phi\phi}\boldsymbol{\phi}_{\mathrm{s}} = \boldsymbol{0} \end{cases} \tag{12}$$

Here $\boldsymbol{M}_{\mathrm{uu}}$, $\boldsymbol{C}_{\mathrm{uu}}$, $\boldsymbol{K}_{\mathrm{uu}}$, $\boldsymbol{K}_{\mathrm{u}\phi}$, $\boldsymbol{K}_{\phi\mathrm{u}}$ and $\boldsymbol{K}_{\phi\phi}$ denote the mass matrix, the damping matrix, the stiffness matrix, the piezoelectric coupled matrix, the coupled capacity matrix and the piezoelectric capacity matrix, respectively. Furthermore, $\boldsymbol{F}_{\mathrm{ue}}$, $\boldsymbol{q}$, $\boldsymbol{\phi}_{\mathrm{a}}$ and $\boldsymbol{\phi}_{\mathrm{s}}$ are the external force vector, the nodal displacement vector, the actuation voltage vector and the sensor voltage vector, respectively. In Eq. (12), $\dot{\square}$ and $\ddot{\square}$ represent the first and second time derivatives. The above system matrices and vectors are calculated by

$$\begin{cases} \boldsymbol{M}_{\mathrm{uu}} = \int_V \rho \boldsymbol{N}_{\mathrm{v}}^{\mathrm{T}} \boldsymbol{Z}_{\mathrm{u}}^{\mathrm{T}} \boldsymbol{Z}_{\mathrm{u}} \boldsymbol{N}_{\mathrm{v}}\, \mathrm{d}V \\ \boldsymbol{K}_{\mathrm{uu}} = \int_V \boldsymbol{B}_{\mathrm{u}}^{\mathrm{T}} \boldsymbol{c} \boldsymbol{B}_{\mathrm{u}} \mathrm{d}V \\ \boldsymbol{K}_{\mathrm{u}\phi} = \boldsymbol{K}_{\mathrm{u}\phi}^{\mathrm{T}} = -\int_V \boldsymbol{B}_{\mathrm{u}}^{\mathrm{T}} \boldsymbol{e}^{\mathrm{T}} \boldsymbol{B}_{\phi}\, \mathrm{d}V \\ \boldsymbol{K}_{\phi\phi} = -\int_V \boldsymbol{B}_{\phi}^{\mathrm{T}} \boldsymbol{\chi} \boldsymbol{B}_{\phi} \mathrm{d}V \\ \boldsymbol{F}_{\mathrm{ue}} = \int_V \boldsymbol{N}_{\mathrm{v}}^{\mathrm{T}} \boldsymbol{Z}_{\mathrm{u}}^{\mathrm{T}} \boldsymbol{f}_{\mathrm{b}} \mathrm{d}V + \int_{\Omega} \boldsymbol{N}_{\mathrm{v}}^{\mathrm{T}} \boldsymbol{Z}_{\mathrm{u}}^{\mathrm{T}} \boldsymbol{f}_{\mathrm{s}}\, \mathrm{d}\Omega \\ \qquad + \boldsymbol{N}_{\mathrm{v}}^{\mathrm{T}} \boldsymbol{Z}_{\mathrm{u}}^{\mathrm{T}} \boldsymbol{f}_{\mathrm{c}} \end{cases} \tag{13}$$

where ρ is the density, $\boldsymbol{N}_{\mathrm{v}}$ the shape function matrix, $\boldsymbol{B}_{\mathrm{u}}$ the strain field matrix and $\boldsymbol{B}_{\phi}$ the electric field matrix. The damp-

ing matrix $\boldsymbol{C}_{\mathrm{uu}}$ is calculated using Rayleigh damping coefficients, computation method, which is linear with respect to mass and stiffness matrices.

3. State space expression

Due to large number of DOFs of the dynamic FE model, a truncated modal matrix[54] $\boldsymbol{S}_{\mathrm{r}}$ including the first r modes is introduced to decompose and reduce the model to avoid high costs of computation time. Therefore, the nodal displacement vector $\boldsymbol{q}$ can be transferred to a modal displacement vector $\boldsymbol{z}_{\mathrm{r}}$ with small number of DOFs as

$$\boldsymbol{q} = \boldsymbol{S}_{\mathrm{r}}\boldsymbol{z}_{\mathrm{r}} \tag{14}$$

Substituting Eq. (14) into Eq. (12) and left-multiplying it by the transposed modal matrix, one obtains the decomposed and reduced equation of motion as

$$\widetilde{\boldsymbol{M}}_{\mathrm{uu}}\ddot{\boldsymbol{z}}_{\mathrm{r}} + \widetilde{\boldsymbol{C}}_{\mathrm{uu}}\dot{\boldsymbol{z}}_{\mathrm{r}} + \widetilde{\boldsymbol{K}}_{\mathrm{uu}}\boldsymbol{z}_{\mathrm{r}} = \boldsymbol{S}_{\mathrm{r}}^{\mathrm{T}}\boldsymbol{F}_{\mathrm{ue}} - \boldsymbol{S}_{\mathrm{r}}^{\mathrm{T}}\boldsymbol{K}_{\mathrm{u}\phi}\boldsymbol{\phi}_{\mathrm{a}} \tag{15}$$

where $\widetilde{\boldsymbol{M}}_{\mathrm{uu}}$, $\widetilde{\boldsymbol{C}}_{\mathrm{uu}}$ and $\widetilde{\boldsymbol{K}}_{\mathrm{uu}}$ are the modal mass, damping and stiffness matrices, respectively, which are diagonal. Again using Eq. (14), the sensor equation given in Eq. (12) can be expressed by modal coordinates as

$$\boldsymbol{\phi}_{\mathrm{s}} = -\boldsymbol{K}_{\phi\phi}^{-1}\boldsymbol{K}_{\phi\mathrm{u}}\boldsymbol{S}_{\mathrm{r}}\boldsymbol{z}_{\mathrm{r}} \tag{16}$$

Defining the state vector $\boldsymbol{x}(t)$, the measured output vector $\boldsymbol{y}(t)$ and the control input vector $\boldsymbol{u}(t)$ as

$$\boldsymbol{x} = \begin{bmatrix} \boldsymbol{z}_{\mathrm{r}} \\ \dot{\boldsymbol{z}}_{\mathrm{r}} \end{bmatrix}, \boldsymbol{y} = \boldsymbol{\phi}_{\mathrm{s}}, \boldsymbol{u} = \boldsymbol{\phi}_{\mathrm{a}} \tag{17}$$

and the dynamic FE model of the smart structure can be expressed in state space form as

$$\begin{cases} \dot{\boldsymbol{x}}(t) = \boldsymbol{A}\boldsymbol{x}(t) + \boldsymbol{B}\boldsymbol{u}(t) \\ \boldsymbol{y}(t) = \boldsymbol{C}\boldsymbol{x}(t) \end{cases} \tag{18}$$

where $\boldsymbol{A}$, $\boldsymbol{B}$ and $\boldsymbol{C}$ denote the system matrix, the control matrix and the system output matrix, respectively. They can be obtained as

$$\begin{cases} \boldsymbol{A} = \begin{bmatrix} \boldsymbol{0} & \boldsymbol{I} \\ -\widetilde{\boldsymbol{M}}_{\mathrm{uu}}^{-1}\widetilde{\boldsymbol{K}}_{\mathrm{uu}} & -\widetilde{\boldsymbol{M}}_{\mathrm{uu}}^{-1}\widetilde{\boldsymbol{C}}_{\mathrm{uu}} \end{bmatrix} \\ \boldsymbol{B} = \begin{bmatrix} \boldsymbol{0} \\ -\widetilde{\boldsymbol{M}}_{\mathrm{uu}}^{-1}\boldsymbol{S}_{\mathrm{r}}^{\mathrm{T}}\boldsymbol{K}_{\mathrm{u}\phi} \end{bmatrix} \\ \boldsymbol{C} = \begin{bmatrix} -\boldsymbol{K}_{\phi\phi}^{-1}\boldsymbol{K}_{\phi\mathrm{u}}\boldsymbol{S}_{\mathrm{r}} & \boldsymbol{0} \end{bmatrix} \end{cases} \tag{19}$$

4. PID control algorithm

PID control can be realized by applying the proportional, integral and derivative of the output error $\boldsymbol{e}(t)$ on actuators, as shown in Fig. 3.

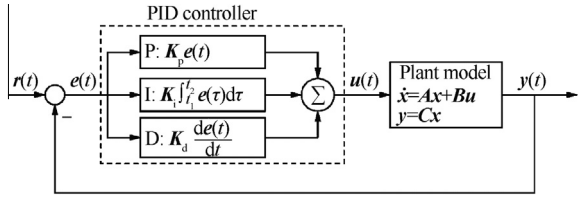

Fig. 3 Sketch of PID feedback control system.

In Fig. 3, we define $\boldsymbol{r}(t)$, $\boldsymbol{y}(t)$, $\boldsymbol{e}(t)$, and $\boldsymbol{u}(t)$ as the reference signal, the measured output, the output error, and the system input (or manipulated variable), respectively. Additionally, the output error is defined as

$$\boldsymbol{e}(t) = \boldsymbol{r}(t) - \boldsymbol{y}(t) \tag{20}$$

According to the strategy of PID control, the control input vector can be defined as a summation of proportional, integral and derivative of output error as

$$\boldsymbol{u}(t) = \boldsymbol{K}_{\mathrm{p}}\boldsymbol{e}(t) + \boldsymbol{K}_{\mathrm{i}}\int_0^t \boldsymbol{e}(\tau)\,\mathrm{d}\tau + \boldsymbol{K}_{\mathrm{d}}\frac{\mathrm{d}\boldsymbol{e}(t)}{\mathrm{d}t} \tag{21}$$

Here, $\boldsymbol{K}_{\mathrm{p}}$, $\boldsymbol{K}_{\mathrm{i}}$ and $\boldsymbol{K}_{\mathrm{d}}$ denote the proportional gain, integral gain and derivative gain, respectively. If only $\boldsymbol{K}_{\mathrm{d}}$ is non-zero and other two gains are zero, the PID control will be reduced to D control. D control with respect to sensor voltage or displacement is equivalent to velocity feedback control, which has been implemented by many researchers. Analogously, neglecting the integral part leads to a PD control law, which considers steady-state error.

In the application of vibration suppression, we need the measured output signal to be zero, meaning that the reference signal is zero here. Therefore, Eq. (20) becomes

$$\boldsymbol{e}(t) = -\boldsymbol{y}(t) = -\boldsymbol{C}\boldsymbol{x}(t) \tag{22}$$

In order to derive the closed-loop system with PID control integrated, a new state variable has to be introduced, which is defined as

$$\boldsymbol{f}(t) = \int_0^t \boldsymbol{y}(\tau)\mathrm{d}\tau \tag{23}$$

Taking the time derivative on both sides yields

$$\dot{\boldsymbol{f}}(t) = \boldsymbol{y}(t) \tag{24}$$

Further substituting Eqs. (22)–(23) into Eq. (21) yields

$$\boldsymbol{u} = -\boldsymbol{K}_{\mathrm{p}}\boldsymbol{C}\boldsymbol{x} - \boldsymbol{K}_{\mathrm{i}}\boldsymbol{f} - \boldsymbol{K}_{\mathrm{d}}\boldsymbol{C}\dot{\boldsymbol{x}} \tag{25}$$

Extending the state variables to

$$\widetilde{\boldsymbol{x}} = \begin{bmatrix} \boldsymbol{x} \\ \boldsymbol{f} \end{bmatrix} \tag{26}$$

the closed-loop state space equations with PID controller can be obtained in terms of the extended state variables as

$$\begin{cases} \dot{\widetilde{\boldsymbol{x}}} = \begin{bmatrix} \widetilde{\boldsymbol{A}}_{11} & \widetilde{\boldsymbol{A}}_{12} \\ \boldsymbol{C} & \boldsymbol{0} \end{bmatrix}\widetilde{\boldsymbol{x}} = \widetilde{\boldsymbol{A}}\widetilde{\boldsymbol{x}} \\ \boldsymbol{y} = [\boldsymbol{C} \quad \boldsymbol{0}]\widetilde{\boldsymbol{x}} \end{cases} \tag{27}$$

with

$$\begin{cases} \widetilde{\boldsymbol{A}}_{11} = (\boldsymbol{I} + \boldsymbol{B}\boldsymbol{K}_{\mathrm{d}}\boldsymbol{C})^{-1}(\boldsymbol{A} - \boldsymbol{B}\boldsymbol{K}_{\mathrm{p}}\boldsymbol{C}) \\ \widetilde{\boldsymbol{A}}_{12} = (\boldsymbol{I} + \boldsymbol{B}\boldsymbol{K}_{\mathrm{d}}\boldsymbol{C})^{-1}(-\boldsymbol{B}\boldsymbol{K}_{\mathrm{i}}) \end{cases} \tag{28}$$

The plant system input signal which is also the output of the PID controller can be calculated by

$$\boldsymbol{u} = (\boldsymbol{I} + \boldsymbol{B}\boldsymbol{K}_{\mathrm{d}}\boldsymbol{C})^{-1}[-(\boldsymbol{K}_{\mathrm{p}}\boldsymbol{C} + \boldsymbol{K}_{\mathrm{d}}\boldsymbol{C}\boldsymbol{A}) \quad -\boldsymbol{K}_{\mathrm{i}}]\widetilde{\boldsymbol{x}} \tag{29}$$

5. LQR optimization method

LQR optimal control, which is a full state feedback control, is briefly introduced for comparison with PID control. An

optimized control gain can be obtained by minimizing the following cost function given as

$$\boldsymbol{J}_{\mathrm{LQR}} = \int_0^{\infty} (\boldsymbol{y}(t)^{\mathrm{T}}\overline{\boldsymbol{Q}}\boldsymbol{y}(t) + \boldsymbol{u}(t)\overline{\boldsymbol{R}}\boldsymbol{u}(t))\,\mathrm{d}t \tag{30}$$

Here, $\overline{\boldsymbol{Q}}$ and $\overline{\boldsymbol{R}}$ are the weighting matrices for the system output and the system input vectors, respectively, which are symmetric positive definite matrices. The weighting matrices can be approximated by Bryson's rule as

$$\overline{Q}_{ii} = \frac{1}{\max(|y_i|^2)} \quad \text{and} \quad \overline{R}_{ii} = \frac{1}{\max(|u_i|^2)} \tag{31}$$

If all the state variables are measured, the control input can be designed as

$$\boldsymbol{u} = -\boldsymbol{K}\boldsymbol{x} \tag{32}$$

with

$$\boldsymbol{K} = \boldsymbol{R}_{\mathrm{r}}^{-1}\boldsymbol{B}^{\mathrm{T}}\boldsymbol{P} \tag{33}$$

Here, the symmetric positive definite matrix $\boldsymbol{P}$ is the solution of the following algebraic Riccati equation as

$$\boldsymbol{A}^{\mathrm{T}}\boldsymbol{P} + \boldsymbol{P}\boldsymbol{A} + \boldsymbol{Q}_{\mathrm{r}} - \boldsymbol{P}\boldsymbol{B}\boldsymbol{R}_{\mathrm{r}}^{-1}\boldsymbol{B}^{\mathrm{T}}\boldsymbol{P} = \boldsymbol{0} \tag{34}$$

with

$$\boldsymbol{Q}_{\mathrm{r}} = \boldsymbol{C}^{\mathrm{T}}\overline{\boldsymbol{Q}}\boldsymbol{C} \quad \textbf{and} \quad \boldsymbol{R}_r = \overline{\boldsymbol{R}} \tag{35}$$

Substituting Eq. (32) into the state space model in Eq. (18) yields the closed-loop system with consideration of LQR controller as

$$\begin{cases} \dot{\boldsymbol{x}} = (\boldsymbol{A} - \boldsymbol{B}\boldsymbol{K})\boldsymbol{x} \\ \boldsymbol{y} = \boldsymbol{C}\boldsymbol{x} \end{cases} \tag{36}$$

6. Active control simulation

6.1. Piezolaminated composite plate

The example for control simulation of smart structures is a cantilevered PZT layered composite plate proposed by Lam et al.,[55] which is shown in Fig. 4.

The cantilevered piezolaminated composite plate consists of one composite master layer, on which two PZT layers with opposite polarizations pointing outward are bonded at the top and bottom surfaces. The host structure is made of T300/976 graphite-epoxy composite material with four substrate layers, the stacking sequence of which is antisymmetric angle-ply [−45/45/−45/45]. The length and width of the composite structure are both 200 mm. The total thickness of the master layer is 1 mm with the thickness of 0.25 mm for each substrate, and the thickness of each PZT layer is 0.1 mm. The material properties of T300/976 composite material are $E_1 = 150$ GPa, $E_2 = 9$ GPa, $G_{12} = G_{13} = 7.1$ GPa, $G_{23} = 2.5$ GPa, $v = 0.3$, $\rho = 1600\ \mathrm{kg/m^3}$, and those for PZT layers are $E = 63$ GPa, $v = 0.3$, $\rho = 7600\ \mathrm{kg/m^3}$, $d_{31} = d_{32} = -2.54\times10^{-12}\mathrm{C/N}$, $\chi_{33} = 1.5\times10^{-8}\mathrm{F/m}$. The smart plate is meshed with 5×5 elements. The damping matrix is obtained by Rayleigh damping coefficient computation method in consideration of the damping ratio of 0.8% for the first six modes.

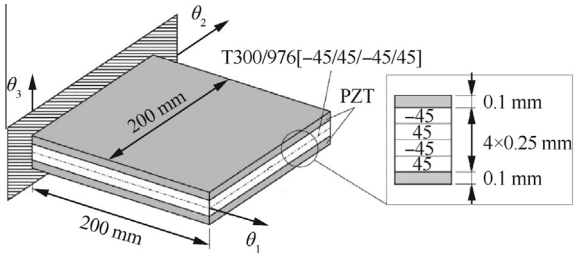

Fig. 4 Piezolaminated composite plate.

In order to validate the present dynamic FE model, the first five eigenfrequencies of the plate are calculated (see Table 1), which implies good agreement with that reported in Ref. [55]

6.2. Control parameters

Due to the large size of the present FE model, the dynamic model is reduced to retain only the first 12 modes for control simulation. The upper PZT layer acts as a sensor, while the lower one acts as an actuator. The control parameters of PID and LQR control strategies are given in Tables 2 and 3. The parameters for LQR control (Case 1) are tuned in order to get the similar vibration effect with D control, and those for the Case 2 are chosen to keep the same maximum control voltage with that obtained from PID control of Case 3. Using these parameters of LQR and PID control, several cases are simulated, including free vibrations and forced vibrations under various excitation forces.

Table 1 The first five eigenfrequencies of piezolaminated plate.

Mode	Eigenfrequency (Hz)		Discrepancy (%)
	Lam et al.[55]	Present	
1	21.4657	21.5083	0.20
2	63.3491	63.2409	0.17
3	130.8221	129.9076	0.79
4	182.4224	183.4276	0.55
5	218.2750	217.8606	0.19

Table 2 PID control parameters.

Control type	K_{p}	K_{i}	K_{d}
D control	0	0	0.01
PD control	2	0	0.01
PID control, Case 1	2	100	0.01
PID control, Case 2	2	100	0.03
PID control, Case 3	2	400	0.03

Table 3 LQR control parameters.

Control type	$\overline{Q}$	$\overline{R}$
LQR control, Case 1	$1/5^2$	$1/8.5^2$
LQR control, Case 2	$1/5^2$	$1/70^2$

6.3. Free vibrations

In the first vibration control simulation, the proposed control strategies are applied to free plate vibrations starting from an initial configuration generated by a uniformly distributed pressure of 100 Pa. The sensor signals and the control input signals are presented in Fig. 5(a) and (b), respectively.

From the results, it can be seen that D control and LQR control of case 1, which will generate similar control input signals, perform similarly on vibration suppression. Adding proportional or proportional-integral effects leads to worse control results using the same derivative gain. This is because free vibrations have no steady-state error. Therefore, the proportional or integral part has no contribution to vibration suppression. In contrast, it will deteriorate the dynamic behavior.

6.4. Step excitation

The second simulation considers the plate excited by a step force 1 N at point A starting from 0.1 s. The uncontrolled/controlled vibrations and the actuation voltage signals are given in Figs. 6 and 7.

From Fig. 6, one can see that D control only damps the free vibration part without counteracting the forced vibration. Analogously, LQR control of case 1 performs similarly to D control, but it will counteract slightly the forced vibration part. Adding the control action of the proportional of steady-state error leads to a PD control, which can counteract the steady-state error. However, PD control cannot completely cancel the steady-state error. Further adding the integral part, the resulting PID control will completely compensate the steady state error in a certain

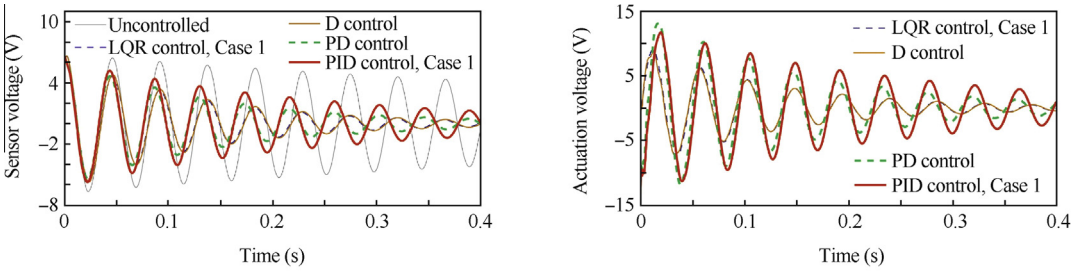

(a) Sensor signals (b) Control input signals

Fig. 5 Dynamic responses of free plate vibrations damped by various control strategies.

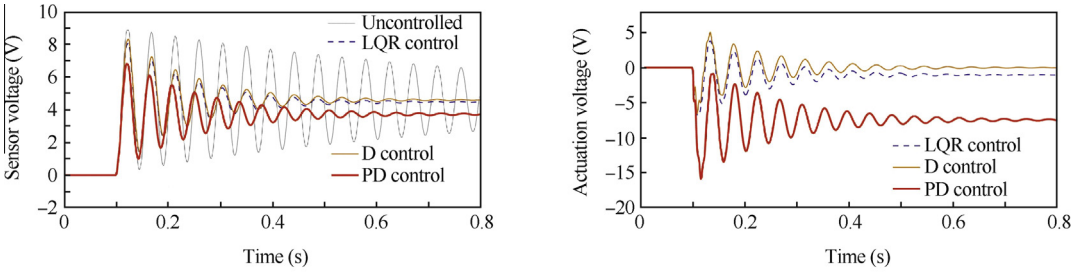

(a) Sensor signals (b) Control input signals

Fig. 6 Dynamic responses of plate by LQR, D and PD control under a step force excitation.

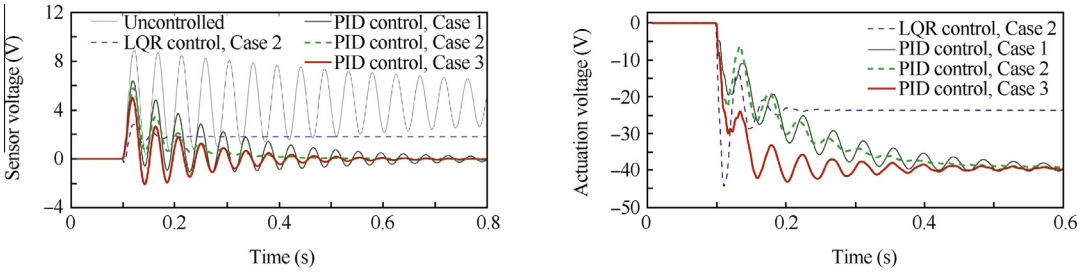

(a) Sensor signals (b) Control input signals

Fig. 7 Dynamic responses of plate by LQR and PID control under a step force excitation.

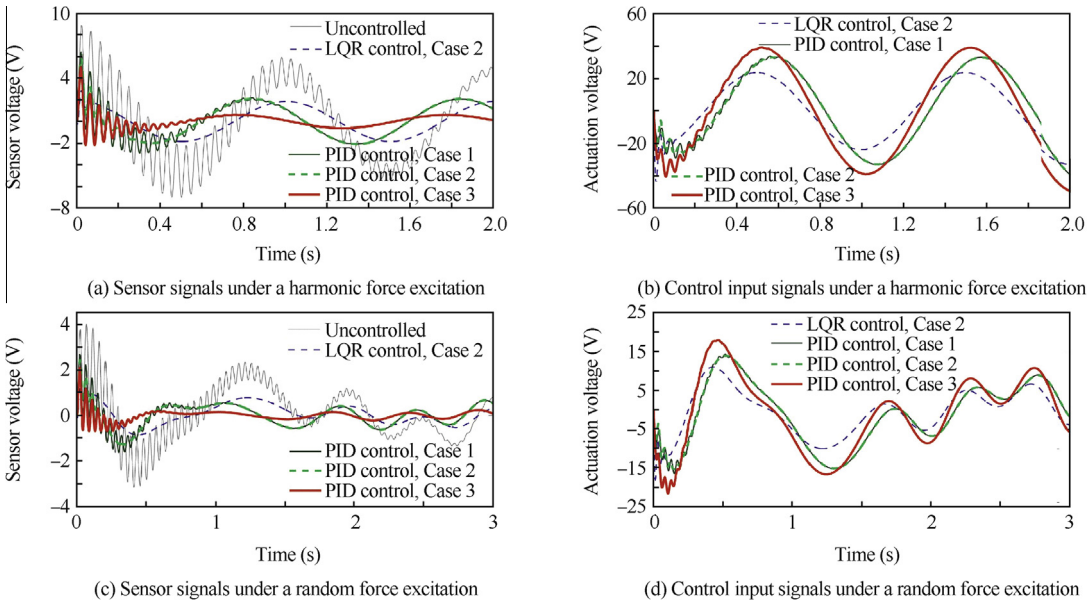

Fig. 8 Dynamic response of plate by LQR and PID control under a harmonic and random force excitations.

period, as shown in Fig. 7. Since the integral control action will increase the overshoot, the free vibration suppressed by PID control of case 1 becomes worse than that by D control. Increasing K_d (PID control of Case 2) will lead to small amplitudes of the free vibration signal due to large control action. To get a fast suppression of vibration in a short period, one can increase K_i, for example from 100 to 400, leading to PID control of case 3. However, even though the maximum control voltage of LQR control reaches as large as that generated by PID of case 3, there still exists steady-state error(see Fig. 7).

6.5. Harmonic excitation

In this application, a harmonic periodical force is considered to excite the plate at point A, generated by the function $f(t) = \cos(2\pi t)$ N. The dynamic response and control input signals are respectively displayed in Fig. 8(a) and (b). The figure illustrates that the vibrations suppressed by PID control of Case 3 have the smallest amplitude among other controllers. PID control of Case 1 and Case 2 performs similarly and the latter one has smaller amplitudes of free vibration. The amplitudes of vibrations suppressed by PID control of Case 3 are smaller than those by LQR control, even though they have similar maximum control voltage appearing in the beginning.

6.6. Random excitation

In the last simulation, a random excitation signal is considered. The results are shown in Fig. 8(c) and (d). Similar control effects like the previous simulations can be observed. The PID control of Case 3 produces the best results compared to other control strategies. PID control of Case 1 and Case 2 are quite similar, both of which suppress the vibration similarly with LQR control of Case 2.

7. Conclusions

(1) D control only counteracts the free vibrations, but has no effect on the steady-state error.
(2) The proportional and integral part will counteract the steady-state error, but have a negative effect on free vibration suppression.
(3) For the forced vibrations, in which both the dynamic and steady-state error exist, PID control gives the best results compared to LQR, D and PD control.

Acknowledgements

This work is partially supported by the National Natural Science Foundation of China (No. 51275413). Furthermore, the authors would like to gratefully acknowledge the financial support from the China Scholarship Council of China for the first author (No. 2010629003).

References

1. Ray MC, Bhattacharya R, Samanta B. Exact solutions for dynamic analysis of composite plates with distributed piezoelectric layers. *Comput Struct* 1998;**66**(6):737–43.
2. Sze KY, Yao LQ. A hybrid stress ANS solid-shell element and its generalization for smart structure modeling: Part I Solid shell element formulation. *Int J Numer Meth Eng* 2000;**48**(4):545–64.
3. He LH. Three dimensional analysis of some symmetric hybrid piezoelectric laminates. *Z Angew Math Mech* 2000;**80**(5):307–18.
4. Kapuria S, Kumari P. Three-dimensional piezoelasticity solution for dynamics of cross-ply cylindrical shells integrated with piezoelectric fiber reinforced composite actuators and sensors. *Compos Struct* 2010;**92**(10):2431–44.
5. Liu X, Chen R, Zhu L. Energy conversion efficiency of rainbow shape piezoelectric transducer. *Chin J Aeronaut* 2012;**25**(5):691–7.

6. Tzou HS, Chai WK. Design and testing of a hybrid polymeric electrostrictive/piezoelectric beam with bang-bang control. *Mech Syst Signal Process* 2007;**21**(1):417–29.
7. Kucuk I, Sadek IS, Zeihi E, Adali S. Optimal vibration control of piezolaminated smart beams by the maximum principle. *Comput Struct* 2011;**89**(9–10):744–9.
8. Narayanan S, Balamurugan V. Finite element modeling of piezolaminated smart structures for active vibration control with distributed sensors and actuators. *J Sound Vib* 2003;**262**(3):529–62.
9. Marinaki M, Marinakis Y, Stavroulakis GE. Vibration control of beams with piezoelectric sensors and actuators using partical swarm optimization. *Expert Syst Appl* 2011;**38**(6):6872–83.
10. Liu GR, Peng XQ, Lam KY, Tani J. Vibration control simulation of laminated composite plates with integrated piezoelectrics. *J Sound Vib* 1999;**220**(5):827–46.
11. Kioua H, Mirza S. Piezoelectric induced bending and twisting of laminated composite shallow shells. *Smart Mater Struct* 2000;**9**(4):476–84.
12. Moita JMS, Correia VMF, Martins PG, Soares CMM, Soares CAM. Optimal design in vibration control of adaptive structures using a simulated annealing algorithm. *Compos Struct* 2006;**75**(1–4):79–87.
13. Kapuria S, Dumir PC. First order shear deformation theory for hybrid cylindrical panel in cylindrical bending considering electrothermomechanical coupling effects. *Z Angew Math Mech* 2002;**82**(7):461–71.
14. Wang SY, Quek ST, Ang KK. Dynamic stability analysis of finite element modeling of piezoelectric composite plates. *Int J Solids Struct* 2004;**41**(3–4):745–64.
15. Zheng SJ. Finite element analysis of smart structures with piezoelectric sensors/actuators including debonding. *Chin J Aeronaut* 2004;**17**(4):246–50.
16. Liu GR, Dai KY, Lim KM. Static and vibration control of composite laminates integrated with piezoelectric sensors and actuators using the radial point interpolation method. *Smart Mater Struct* 2004;**13**(6):1438–47.
17. Marinković D, Köppe H, Gabbert U. Accurate modeling of the electric field within piezoelectric layers for active composite structures. *J Int Mat Syst Str* 2007;**18**(5):503–13.
18. Zhang SQ, Schmidt R. Large rotation FE transient analysis of piezolaminated thinwalled smart structures. *Smart Mater Struct* 2013;**22**(10):105025.
19. Zhang SQ, Schmidt R. Large rotation theory for static analysis of composite and piezoelectric laminated thin-walled structures. *Thin Wall Struct* 2014;**78**:16–25.
20. Zhang SQ, Schmidt R. Static and dynamic FE analysis of piezoelectric integrated thin-walled composite structures with large rotations. *Compos Struct* 2014;**112**:345–57.
21. Shimpi RP, Patel HG. Free vibration of plate using two variable refined plate theory. *J Sound Vib* 2006;**296**(4–5):979–99.
22. Reddy JN. A general non-linear third-order theory of plates with moderate thickness. *Int J Nonlin Mech* 1990;**25**(6):677–86.
23. Hanna NF, Leissa AW. A higher order shear deformation theory for the vibration of thick plates. *J Sound Vib* 1994;**170**(4):545–55.
24. Correia VMF, Gomes MAA, Suleman A, Soares CMM, Soares CAM. Modelling and design of adaptive composite structures. *Comput Method Appl M* 2000;**185**(2–4):325–46.
25. Moita JS, Martins PG, Soares CMM, Soares CAM. Optimal dynamic control of laminated adaptive structures using a higher order model and a genetic algorithm. *Comput Struct* 2008;**86**(3–5):198–206.
26. Schmidt R, Vu TD. Nonlinear dynamic FE simulation of smart piezolaminated structures based on first- and third-order transverse shear deformation theory. *Adv Mater Res* 2009;**79–82**:1313–6.
27. Vasques CMA, Rodrigues JD. Coupled three-layered analysis of smart piezoelectric beams with different electric bounday conditions. *Int J Numer Meth Eng* 2005;**62**(11):1488–518.
28. Kapuria S. An efficient coupled theory for multilayered beams with embedded piezoelectric sensory and active layers. *Int J Solids Struct* 2001;**38**(50–51):9179–99.
29. Kapuria S, Dumir PC, Ahmed A. An efficient coupled layerwise theory for dynamic analysis of piezoelectric composite beams. *J Sound Vib* 2003;**261**(5):927–44.
30. Tzou HS, Tseng CI. Distributed modal identification and vibration control of continua: Piezoelectric finite element formulation and analysis. *J Dyn Syst-T ASME* 1991;**113**(3):500–5.
31. Kang YK, Park HC, Kim J, Choi SB. Interaction of active and passive vibration control of laminated composite beams with piezoelectric sensors/actuators. *Mater Des* 2002;**23**:277–86.
32. Balamurugan V, Narayanan S. Shell finite element for smart piezoelectric composite plate/shell structures and its application to the study of active vibration control. *Finite Elem Anal Des* 2001;**37**(9):713–38.
33. Kumar R, Mishra BK, Jain SC. Static and dynamic analysis of smart cylindrical shell. *Finite Elem Anal Des* 2008;**45**(1):13–24.
34. Sheng GG, Wang X. Active control of functionally graded laminated cylindrical shells. *Compos Struct* 2009;**90**(4):448–57.
35. Zhang X, Kang Z. Topology optimization of piezoelectric layers in plates with active vibration control. *J Int Mat Syst Str* 2013;**25**(6):697–712.
36. Kulkarni SA, Bajoria KM. Finite element modeling of smart plates/shells using higher order shear deformation theory. *Compos Struct* 2003;**62**(1):41–50.
37. Ray MC, Reddy JN. Active control of laminated cylindrical shells using piezoelectric fiber reinforced composites. *Compos Struct* 2005;**65**(7–8):1226–36.
38. Vasques CMA, Rodrigues JD. Active vibration control of smart piezoelectric beams: comparison of classical and optimal feedback control strategies. *Comput Struct* 2006;**84**(22–23):1402–14.
39. Malgaca L. Integration of active vibration control methods with finite element models of smart laminated composite structures. *Compos Struct* 2010;**92**(7):1651–63.
40. Zhang SQ, Schmidt R. LQR control for vibration suppression of piezoelectric integrated smart structures. *Proc Appl Math Mech* 2012;**12**(1):695–6.
41. Valliappan S, Qi K. Finite element analysis of a 'smart' damper for seismic structural control. *Comput Struct* 2003;**81**(8–11):1009–17.
42. Xu SX, Koko TS. Finite element analysis and design of actively controlled piezoelectric smart structures. *Finite Elem Anal Des* 2004;**40**(3):241–62.
43. Dong XJ, Meng G, Peng JC. Vibration control of piezoelectric smart structures based on system identification technique: numerical simulation and experimental study. *J Sound Vib* 2006;**297**(3–5):680–93.
44. Stavroulakis GE, Foutsitzi G, Hadjigeorgiou E, Marinova D, Baniotopoulos CC. Design and robust optimal control of smart beams with application on vibrations suppression. *Adv Eng Softw* 2005;**36**(11–12):806–13.
45. Roy T, Chakraborty D. Optimal vibration control of smart fiber reinforced composite shell structures using improved genetic algorithm. *J Sound Vib* 2009;**319**(1–2):15–40.
46. Chen CQ, Shen YP. Optimal control of active structures with piezoelectric modal sensors andactuators. *Smart Mater Struct* 1997;**6**(4):403–9.
47. Lin JC, Nien MH. Adaptive control of a composite cantilever beam with piezoelectric dampingmodal actuators/sensors. *Compos Struct* 2005;**70**(2):170–6.
48. Bhattacharya P, Suhail H, Sinha PK. Finite element analysis and distributed control of laminated composite shells using LQR/IMSC approach. *Aerosp Sci Technol* 2002;**6**(4):273–81.
49. Manjunath TC, Bandyopadhyay B. Vibration control of Timoshenko smart structures using multirate output feedback based discrete sliding mode control for SISO systems. *J Sound Vib* 2009;**326**(1–2):50–74.

50. Zhang SQ, Li HN, Schmidt R, Müller PC. Disturbance rejection control for vibration suppression of piezoelectric laminated thin-walled structures. *J Sound Vib* 2014;**333**(5):1209–23.
51. Li P, Cheng L, Li YY, Chen N. Robust control of a vibrating plate using μ-synthesis approach. *Thin Wall Struct* 2003;**41**(11):973–86.
52. Marinova DG, Stavroulakis GE, Zacharenakis C. Robust control of smart beams in the presence of damage-induced structural uncertainties. *Proceedings of international conference on physics and control*; 2005. p. 339–44.
53. Librescu L. *Elastostatics and kinetics of anisotropic and heterogeneous shell-type structures*. Leyden: Noordhoff International; 1975.
54. Piefort V. Finite element modeling of piezoelectric active structures dissertation. Bruxelles: Universite Libre de Bruxelles; 2001.
55. Lam KY, Peng XQ, Liu GR, Reddy JN. A finite-element model for piezoelectric composite laminates. *Smart Mater Struct* 1997;**6**(5):583–91.

Zhang Shunqi is a research assistant at the Institute of General Mechanics, RWTH Aachen University, Germany. He received the B.S. and M.S. degrees in mechanical engineering from Northwestern Polytechnical University, China, in 2007 and 2010 respectively, and then obtained the Ph.D. degree from RWTH Aachen University, Germany, in 2014. His main research interests are structural mechanics, smart structures, composite structures, computational solid mechanics, and active vibration control.

Rüdiger Schmidt is a professor at the RWTH Aachen University. He received his Diploma from RWTH Aachen University in 1973 and got his Ph.D. degree from Ruhr-University Bochum, Germany, in 1981. He finished the Habilitation for professorship at the University of Wuppertal, Germany, in 1992. His area of research includes structural mechanics, smart structures, composite structures, plate and shell theories and computational mechanics.

Qin Xiansheng is a professor and Ph.D. supervisor at the School of Mechanical Engineering, Northwestern Polytechnical University, China. He received the B.S., M.S. and Ph.D. degrees from Northwestern Polytechnical University in 1983, 1986 and 1991, respectively. His current research interests are advanced mechatronical systems and equipment, mechatronical control and automation, as well as computer numerical control systems.